# Liquid Crystals from Polymer-Functionalized $TiO_2$ Nanorod Mesogens

**S. Meuer,[†] K. Fischer,[‡] I. Mey,[‡] A. Janshoff,[‡] M. Schmidt,[‡] and R. Zentel*,[†]**

*Institute for Organic Chemistry, University of Mainz, Duesbergweg 10-14, 55128 Mainz, Germany, and Institute for Physical Chemistry, University of Mainz, Jakob Welder Weg 11, 55128 Mainz, Germany*

*Received June 18, 2008; Revised Manuscript Received August 18, 2008*

ABSTRACT: In this work, we functionalized $TiO_2$ nanorods with dopamine-functionalized diblock copolymers. After functionalization, they are well dispersible in organic solvents. Light scattering proves that the nanorods are dispersed as single objects, and we could use AFM (tapping mode) to visualize the homogeneous polymer shell around the nanorods. When using a LCST polymer such as poly(diethylene glycol monomethyl ether) methacrylate (PDEGMEMA), the functionalized nanorods showed a temperature-dependent dispersion stability. The dispersions became microscopically (light scattering) and macroscopically (turbidity measurement) unstable when reaching the LCST of PDEGMEMA. After investigation of the nanorod mesogens, we investigated their liquid crystalline behavior. The phase diagram of PMMA-functionalized nanorods in PEG 400 as the mobile matrix was explored, and we found a rising clearing temperature with increasing volume fractions of nanorods. On the other hand, we investigated PDEGMEMA-functionalized nanorods in excess PDEGMEMA polymer as the matrix and found again liquid crystalline phases.

## Introduction

The use of nano-objects in the real macroscopic world also requires their macroscopic organization, which can be realized in lyotropic liquid crystals (LC).[1] Generally, the formation of lyotropic liquid crystals[2−4] from rigid-rod objects as a result of form-anisotropy is well understood,[5,6] and such phases offer the potential to orient anisotropic nanoparticles. In this respect, the orientation of functional semiconducting nanoparticles is interesting for materials science and especially for photovoltaics.[7−10] As an example, oriented semiconducting materials might improve the device performance in solar cells by alignment of electron-carrying nanorods perpendicular to the electrode.[11] Following this concept, it was shown by Alivisatos and coworkers that the efficiency of nanoparticle solar cells could be enhanced, if rod-shaped particles are chosen.[12] Research in this direction is, so far, limited by the solubility of functional nanoparticles, which is needed to obtain the LC-phase at high concentration.

Historically lyotropic LC-phases in water have been observed for various rigid-rod objects such as $V_2O_5$ ribbons,[13,14] tobacco mosaic viruses,[15] and $TiO_2$ nanorods,[16] but the charges used to stabilize these systems disable any electronic use. Therefore, ion free mineral liquid crystals from uncharged anisotropic nanoparticles in organic solvents are needed. This requires the "solubilization" of the nano-objects in organic solvents. For this purpose, the particles have to be surface functionalized with a soluble corona to overcome the strong adhesion forces among them.[17,18] The concept of "hairy rods", which was originally developed for stiff main chain liquid crystalline polymers, is very promising for such inorganic nano-objects too.[2] In that concept, a stiff insoluble core is solubilized by linking long chains (the hairs) on its surface. Alkyl chains are often used[19,20] to stabilize nanoparticles of sphere- or rod-like shape, and they are also used for delaminated clay fragments.[21] In some cases, they allow the preparation of highly concentrated solutions, which give rise to a liquid crystalline ordering, if anisotropic nanoparticles are used.

Polymeric surfactants[18,21,22] offer advantages here for the solubilization of inorganic nano-objects: polymers themselves are objects of nanometer dimensions. Therefore, polymer-coated surfaces are stabilized sterically up to a distance of nanometers and not just for angstroms as with alkyl chains. In addition, new polymers designed for surface functionalization have multiple anchor units for surface attachment. Therefore, adsorption−desorption equilibria reactions are avoided, and a robust fixation of the multidentate polymer ligand to the surface can be achieved.

In general, both approaches using small molecules and polymers for the stabilization of nanoparticles lead to soluble and highly mobile systems.[19−23] Liquid crystalline phases of both surfactant and polymer-stabilized nanorods have been found so far, but polymers offer two major advantages as compared to small molecular surfactants: Polymers can be prepared with additional complex functions as stimuli responsive behavior or conductive properties. On the other hand, polymer-functionalized nanoparticles can be incorporated into polymer matrices, which is not possible for surfactant-stabilized systems as they are usually expelled from the polymer matrix. This has been shown for $TiO_2$ nanorods functionalized by random P(MMA-*co*-MA) copolymers. They could be incorporated homogeneously into PMMA films that showed interesting optical properties.[23]

We wanted to focus on the functionalization with well-defined block copolymers where all anchor units are localized in one block. Thus, polymer-driven cross-linking and aggregation of nanorods can be avoided, and the soluble block is fully unfolded into the surrounding solvent, enhancing the steric stabilization. Using this concept, we recently demonstrated the formation of liquid crystalline phases in highly concentrated solutions of $TiO_2$ nanorods.[18] This concept could also be applied successfully to carbon nanotubes.[24] In addition, we were able to solubilize and organize $TiO_2$ nanorods in an organic hole conducting matrix.[25] While, so far, the self-assembly is known, little is known about the individual solubilized nanoparticles (the mesogens) and the details of the formation of the LC-phase.

In this work, we focus on the detailed investigation of the individual $TiO_2$ nanorods functionalized with polymethyl methacrylate (PMMA) and "stimuli responsive" poly(diethylene glycol monomethyl ether) methacrylate (PDEGMEMA) block copolymers. We characterized the functionalized nanorods by light scattering methods and AFM. In addition, we were interested in the origin of the thermotropic phase behavior found before,[18] which cannot be explained by a simple hard rod

* To whom correspondence should be addressed. E-mail: zentel@uni-mainz.de.
[†] Institute for Organic Chemistry, University of Mainz.
[‡] Institute for Physical Chemistry, University of Mainz.

10.1021/ma801369w CCC: $40.75 
Published on Web 10/08/2008

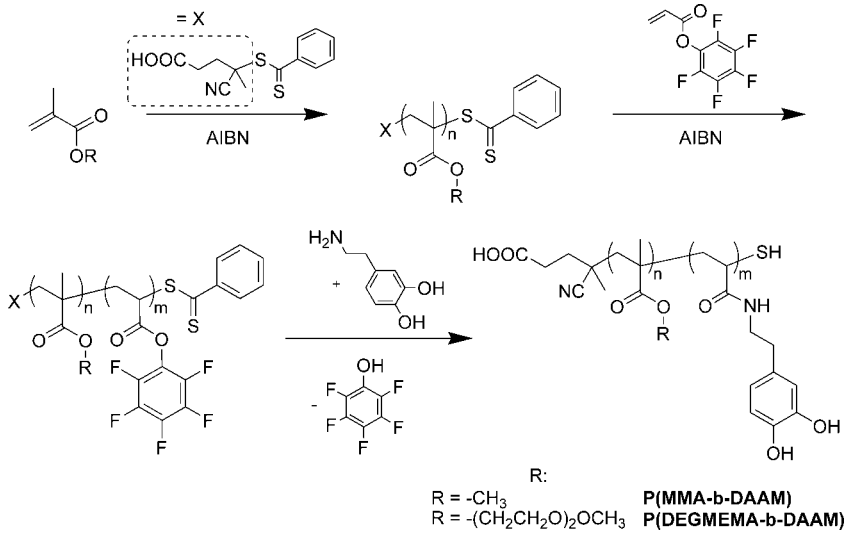


**Figure 1.** Diblock copolymer synthesis.

**Table 1. Polymer Characterization and Adsorption Behavior**

| name | $M_n$/g mol$^{-1}$[a] | PDI[a] | soluble units | anchor units | $N_{chains}$[b] | $A_{chain}$/ nm$^2$[b] |
|---|---|---|---|---|---|---|
| P(MMA-*b*-DAAM) | 12 800 | 1.17 | 66 | 30 | 85 | 13 |
| P(DEGMEMA-*b*-DAAM) **1** | 14 500 | 1.21 | 44 | 30 | 90 | 12 |
| P(DEGMEMA-*b*-DAAM) **2** | 47 500 | 1.53 | 186 | 60 | 9 | 127 |

[a] Determined by GPC (THF). [b] Calculated from TGA experiments.

interaction, and investigated the phase diagram of PMMA-functionalized nanorods in PEG 400.

## Synthesis

**Polymer Synthesis.** The polymers used in this work were prepared via RAFT polymerization. This controlled radical polymerization technique allows the sequential buildup of diblock copolymers with rather narrow polydispersities.[26,27] We used methyl methacrylate as well as (diethylene glycol monomethyl ether) methacrylate as soluble block. Polymers made from these monomers are well soluble in THF, chloroform, and dioxane. Poly (diethylene glycol monomethyl ether) methacrylate (PDEGMEMA) is also soluble in polar solvents like alcohols and has a lower critical solution temperature in water around 25 °C. For the interaction with the nanorod surface, we used the well-investigated anchor unit dopamine. It is found highly exposed in natural adhesion proteins from mussels and binds very strongly to oxidic surfaces.[28] To incorporate this unit into the polymer, we used a reactive ester monomer, which is stable during polymerization and can be reacted with a primary amine polymer-analogous (see Figure 1).[27] The amide is formed quantitatively, and all side products can be removed by repeated precipitation of the polymer solution.

The resulting diblock copolymers poly (methyl methacrylate-*b*-dopamine acryl amide) (P(MMA-*b*-DAAM)) and poly ((diethylene glycol monomethyl ether) methacrylate-*b*-dopamine acryl amide) (P(DEGMEMA-*b*-DAAM)) could be prepared with molecular weights and polydispersities (PDI) reported in Table 1.

The PDIs for the polymer-analogously modified diblock copolymers P(MMA-*b*-DAAM) and P(DEGMEMA-*b*-DAAM) **1** were around 1.2, which is fairly low. The PDI for P(DEGMEMA-b-DAAM) **2** is larger with 1.5, which might be due to diethylene glycol dimethacrylate impurities from the monomer synthesis, which act as cross-linker. This is especially critical if larger blocks are prepared as the probability for interpolymer cross-linking (by incorporation of the same cross-linking monomer in two growing polymer chains) increases dramatically with the block length.

**$TiO_2$ Nanorods.** The $TiO_2$ nanorods used in this work were synthesized with a hydrothermal method that was published before[18] and were used without further modification. Their aspect ratio is stable around 5.5, but their absolute length is rather polydisperse with an average length $\langle L_n \rangle$ of 71 nm and $\langle L_w \rangle$ of 90 nm, resulting in a polydispersity index ($\langle L_w \rangle / \langle L_n \rangle$) of 1.3. To obtain this distribution, we analyzed 350 rods from SEM and TEM images and used the distribution to calculate the average surface per nanorod to be 3800 nm$^2$ and their average volume to be 15 000 nm$^3$. With these values and the known density of rutile (4260 kg/m$^3$), one can calculate the surface and the number of rods present per milligram of powder to $\langle s \rangle_{1mg} = 9.6 \times 10^{16}$ nm$^2$ and $\langle N \rangle_{1mg} = 8.8 \times 10^{13}$.

**Polymer-Functionalized Nanorods.** The functionalization (grafting-to) is done in dilute solution (both polymer and nanorods, see Experimental Section) to prevent interparticle cross-linking. As we start from a dried powder of nanorods, ultrasound treatment is necessary to break the aggregates. This is unfortunately incomplete, so that filtration (0.2 $\mu$m, syringe filter) is necessary to remove unbroken aggregates (around 10 wt %). Bidentate ligands containing enediol moieties such as dopamine serve as robust anchor groups to many metal oxides,[29] and it has been proven spectroscopically that such ligands convert the under-coordinated surface sites back to a bulk-like lattice structure, which results in a really robust binding.[30] Unbound polymer was removed by repeated washing with fresh solvent, and the amount of bound polymer was measured using thermogravimetry (TGA). The samples were heated to 800 °C under a nitrogen atmosphere, and the weight loss was measured as a function of temperature. As $TiO_2$ withstands these temperatures, the weight loss is only due to the decomposition of the polymer (usually by depolymerization). With known molecular weight (see Table 1) and nanorod surface (see section "$TiO_2$ Nanorods"), it is possible to calculate roughly the number of polymer chains that bound per nanorod and the corresponding surface area per chain (see Table 1). The values for P(MMA-*b*-DAAM) and P(DEGMEMA-*b*-DAAM) **1** are quite similar with roughly 90 chains per nanorod and an area of 12 nm$^2$ per polymer chain. The coverage of P(DEGMEMA-b-DAAM) **2** is much smaller, and only about 9 polymer chains are bound to the surface, corresponding to an area of approximately 130 nm$^2$. The lower grafting density of P(DEGMEMA-*b*-DAAM) **2** results, most probably, from two effects. First, the larger soluble

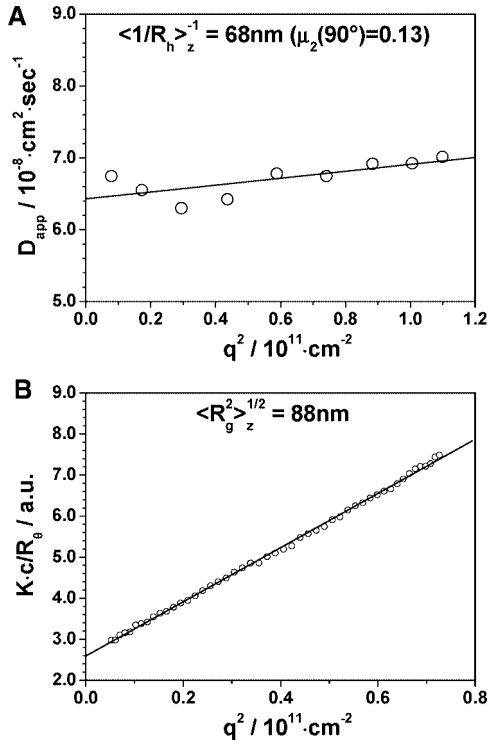


**Figure 2.** (A) Dynamic and (B) static light scattering of P(MMA-*b*-DAAM)-functionalized $TiO_2$ nanorods.

block makes it more difficult to approach the nanorods, and, second, the larger anchor block occupies a larger part of the nanorod surface. Both effects reduce the ability of this diblock copolymer P(DEGMEMA-*b*-DAAM) **2** to bind to the nanorods surface. For P(MMA-*b*-DAAM) and P(DEGMEMA-*b*-DAAM) **1**, both the lengths of the soluble and anchor block are more efficient and the surface area per chain is much smaller than $\pi$ times $R_g^2$ (around 41 nm$^2$ for P(MMA-*b*-DAAM) and around 26 nm$^2$ for P(DEGMEMA-*b*-DAAM) **1**). This can be explained by the formation of a brushlike orientation of the polymers on the nanoparticle surface. P(DEGMEMA-*b*-DAAM) **2** does not form a brushlike layer on the nanorods, but more a dense packing of random coils (also called mushroom-like layer) as the surface area per chain (127 nm$^2$) is almost the same as $\pi$ times $R_g^2$, which is 110 nm$^2$ in this case. In all cases, the surface is covered with a dense polymer layer, leading to good solution stability in suitable solvents for the soluble block.

### Characterization of the Functionalized Nanorods

**PMMA-Functionalized $TiO_2$ Nanorods.** The P(MMA-*b*-DAAM)-functionalized $TiO_2$ nanorods were investigated by dynamic and static light scattering to determine the microscopic dimensions, which provide information on the stability and aggregation of the dispersed nanorods. Because $TiO_2$ has an extremely large refractive index increment, a highly diluted dispersion of $c = 4.5 \times 10^{-5}$ g/L in THF containing $10^{-3}$ M LiBr was utilized. The results are shown in Figure 2, yielding a hydrodynamic radius $\langle 1/R_h \rangle_z^{-1} = 68$ nm and a radius of gyration $\langle R_g^2 \rangle_z^{1/2} = 88$ nm. It is to be noted that due to the large scattering contrast of $TiO_2$ the radius of gyration resembles the pure $TiO_2$ dimension (i.e., the contribution of the anchored polymer chains can be neglected). In contrast, the hydrodynamic radius also contains significant contributions of the anchored polymer chains, which increase the hydrodynamic friction although being optically invisible.

Both radii (68 and 88 nm) are in the vicinity of the number average length of the rods ($L_n = 70$ nm). However, the ratio between both radii and $L_n$ is not as expected from theory, as for monodisperse rods $R_g = 1/\sqrt{12} \cdot L$ ($R_{g,theory} = 20$ nm). As the nanorods used are highly polydisperse, this must be taken into account: We modified the known equations of the *z*-averaged radius of gyration and hydrodynamic radius and implanted a Schulz−Flory or Schulz−Zimm distribution function.[31] Although there is no particular justification to assume a Schulz−Flory or Schulz−Zimm length distribution, it is well-known that for a given polydispersity the shape of the distribution function has little influence (usually less than experimental error) on the relation between *z*-averaged and number averaged quantities. Therefore, the distribution utilized should demonstrate that principally the results can be explained by a certain length distribution. Furthermore, we modified the equation for our nanorod problem: The mass of a nanorod scales with length times width squared, which can be simplified for stable aspect ratios (length/width; in our case around 5.5) to length cubed. These equations can be solved for these simple distribution functions (see Supporting Information) and show the following: the proportionality factor between $\langle R_g^2 \rangle_z^{1/2}$ and $\langle L_n \rangle$ becomes significantly larger, that is, 1.1 for a Schulz−Flory ($L_w/L_n = 2$) and 0.8 for a Schulz−Zimm ($L_w/L_n = 1.5$) distribution. The experimentally observed value of 1.2 suggests that the length distribution in solution is significantly broader as compared to the TEM analysis. For the quantitative analysis of the hydrodynamic radius, the contribution of the polymer shell to the length as well as to the effective hydrodynamic cross-section of the cylinders has to be known. Estimating the hydrodynamic contribution of the soluble PMMA chains to be in the order of the end-to-end distance $\langle R^2 \rangle^{1/2} = 5$ nm, the hydrodynamic radius may be calculated as

$$\langle 1/R_h \rangle_z^{-1} = F(L_n + 2\langle R^2 \rangle^{1/2})/(2\ln(L_n + 2\langle R^2 \rangle^{1/2})/(d + 2\langle R^2 \rangle^{1/2}) + \gamma) \quad (1)$$

with $\langle 1/R_h \rangle_z^{-1}$ the *z*-average of the hydrodynamic radius, $F$ a factor resembling the impact of the length distribution function with $F = 3$ for a Schulz−Flory and $F = 7/3$ for a Schulz−Zimm distribution (see Supporting Information), $L_n$ the number average of the nanorod length, $\langle R^2 \rangle^{1/2}$ the average end-to-end distance of a polymer coil, $d$ the average width of the nanorods, and $\gamma$ a numerical correction factor.

Because $L/d$ does not change with $L$, the logarithmic term is not independent of $L$ anymore. However, because the variation of the aspect ratio introduces a logarithmic correction, only, the value for the aspect ratio $(L_n + 2\langle R^2 \rangle^{1/2})/(d + 2\langle R^2 \rangle^{1/2})$ is fixed to 3.5. Utilizing $\gamma = 0.38$,[32] the experimental $R_h$-value of 68 nm is slightly smaller than that calculated for a Schulz−Flory distribution ($R_h = 73.5$ nm) but significantly larger than that calculated for a Schulz−Zimm distribution ($R_h = 57$ nm; see Supporting Information).

It should be mentioned that the value of the second cumulant $\mu_2 = 0.13$ (determined at 90° scattering angle) also indicates a larger polydispersity of the particles in solution as compared to the TEM analysis. Nevertheless, the results from the scattering experiments show that the polymer-functionalized rods are dispersed as individual objects, indicating a successful stabilization of the $TiO_2$ nanorods by the block copolymer.

**PDEGMEMA-Functionalized $TiO_2$ Nanorods.** PDEGMEMA is a polymer with interesting properties: it has a low glass transition temperature around 0 °C and is a honey-like viscous fluid at room temperature. In addition, it offers solubility not only in THF, chloroform, etc., but also in alcohols and water. In the latter solvent, a lower critical solution temperature (LCST) is found around 20−25 °C (depending on the molecular weight).[33] Below that temperature, the polymer is completely soluble, but rapidly starts to precipitate when raising the

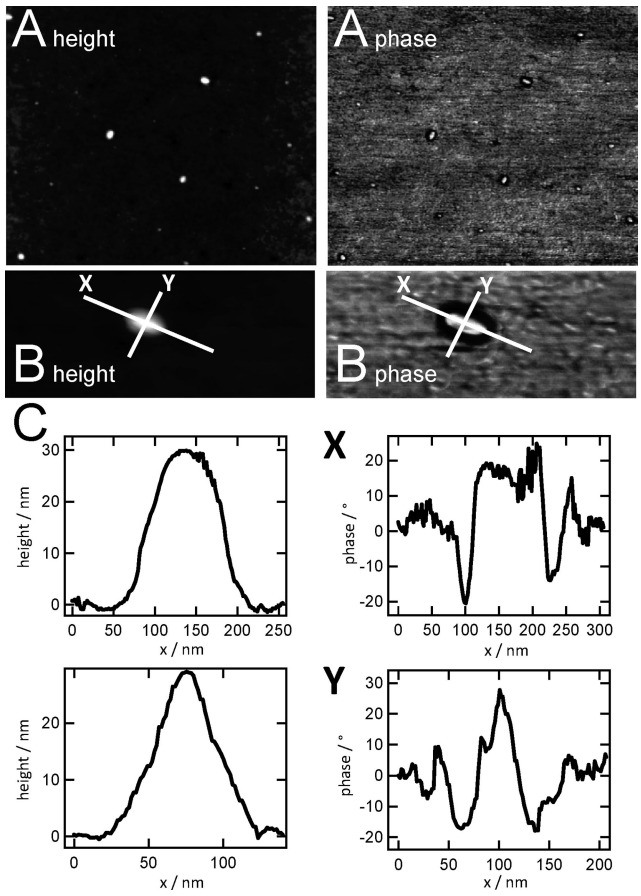


**Figure 3.** AFM images taken in tapping mode. Height and phase image of (A) several P(DEGMEM-*b*-DAAM)-functionalized nanorods, and (B) a single P(DEGMEM-*b*-DAAM)-functionalized nanorod. (C) Line scans along the axes *X* and *Y* marked in Figure 3B.

temperature above the LCST. We used this phenomenon later to switch the dispersions.

Yet in a first experiment, we used the low $T_g$-value of PDEGMEMA to visualize the hard $TiO_2$ core in the soft polymer matrix by AFM "tapping mode" imaging. In this method, the AFM tip is vibrating while scanning the surface. Thus, one can record additionally to the height of the sample the phase shift in the tip frequency, which is dependent on the viscoelastic behavior of the sample. Thus, the soft polymeric P(DEGMEMA-*b*-DAAM) shell around the nanorods should give a nice contrast in the phase image, whereas the height image should show no difference between core and shell. Figure 3 shows the AFM images of P(DEGMEMA-*b*-DAAM) **1**-functionalized nanorods in tapping mode. Line scans along the nanorods are also shown for the height and phase close-up image.

Figure 3 shows AFM images of $TiO_2$ nanoparticles on $SiO_2$ surface obtained in tapping mode at air. Figure 3A show several nanoparticles on the surface, and a close-up of a single nanorod is shown in Figure 3B. In the phase image, a halo around the particle is visualized contributing to energy loss due to increased contact area of the cantilever and to the viscoelastic properties of the polymer coating of the nanoparticles. The available aspect ratio is lower than expected (around 3, expected 5.5 from the starting material), which might be due to sample−tip interactions resulting in a broadening of the nanorod width and length. This effect is usually in the range of nanometers as the tip diameter is around 7−10 nm. The length (e.g., 70 nm) is therefore not affected too much, but the width (e.g., 13 nm) is almost doubled, leading to a much smaller observable aspect ratio.

To investigate the LCST switching behavior of P(DEGMEMA-*b*-DAAM)-functionalized $TiO_2$ nanorods in water, we

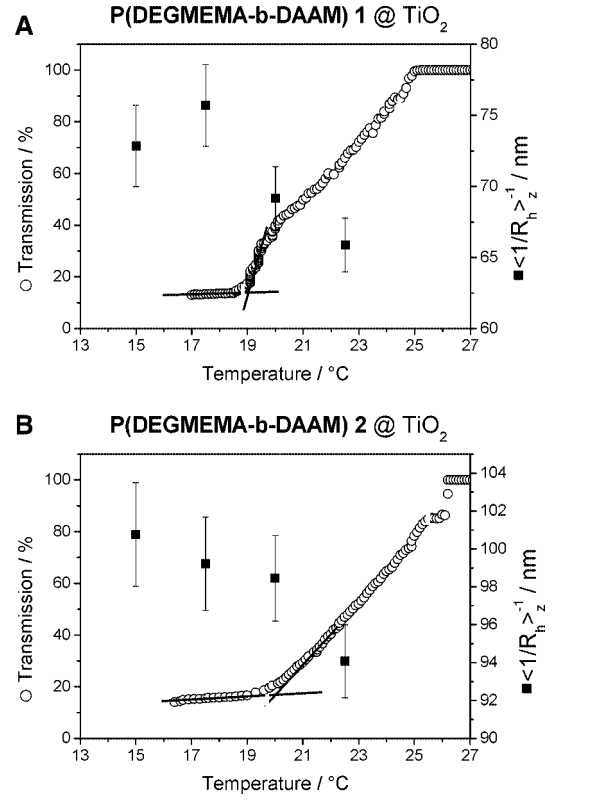


**Figure 4.** Overlaid turbidity measurement (○, left coordinate) and measured $\langle 1/R_h \rangle_z^{-1}$ (■, right coordinate, determined by dynamic light scattering) of (A) P(DEGMEMA-*b*-DAAM) **1**- and (B) P(DEGMEMA-*b*-DAAM) **2**-functionalized $TiO_2$ nanorods.

combined two experiments. First, we prepared a concentrated dispersion (5 mg/mL), which is opaque, and measured the turbidity as a function of temperature. As we start from an opaque dispersion, the measured transmission of light is poor and increases as the dispersion is broken at the LCST followed by sedimentation of the very heavy ($d_{TiO_2}$ = 4.2 g/cm$^3$) aggregates. Second, we measure dynamic light scattering from highly dilute dispersions (0.02 mg/mL, $10^{-3}$ M NaCl in water, PTFE/LG filtered) at various temperatures. The hydrodynamic radius ($\langle 1/R_h \rangle_z^{-1}$) is calculated for each temperature and should get smaller when approaching the LCST. As this is accompanied by precipitation, the measurements were carried out below the LCST to avoid the much stronger scattering of aggregates. The overlaid results of both experiments are shown in Figure 4. We made both experiments for P(DEGMEMA-*b*-DAAM) **1**- and **2**-functionalized $TiO_2$ nanorods to investigate the effect of different grafting densities.

The experiments show three zones: the first zone well below the LCST, the second zone starts around 19 °C for P(DEGMEMA-*b*-DAAM) **1** and around 20 °C for P(DEGMEMA-*b*-DAAM) **2**, and the third zone well above the first two zones. In the first zone, the dispersions are stable macroscopically, and dynamic light scattering shows nicely dispersed single nanorods with a maximal hydrodynamic radius. This indicates that the nanorods are well stabilized on the microscopic scale. In the second zone, the interaction of the polymer with the solvent gets poorer. In dynamic light scattering, the hydrodynamic radius of the individual nanorods starts to decrease, and the first aggregates are formed. Thus, the auto correlation function had to be baseline corrected. At the same time, the concentrated solution becomes less scattered, because the heavy aggregates ($d_{TiO2}$ = 4.2 g/cm$^3$) start to sediment. In the third zone, the dispersions are broken macroscopically (complete sedimentation of large aggregates, leading to clear supernatant liquor).

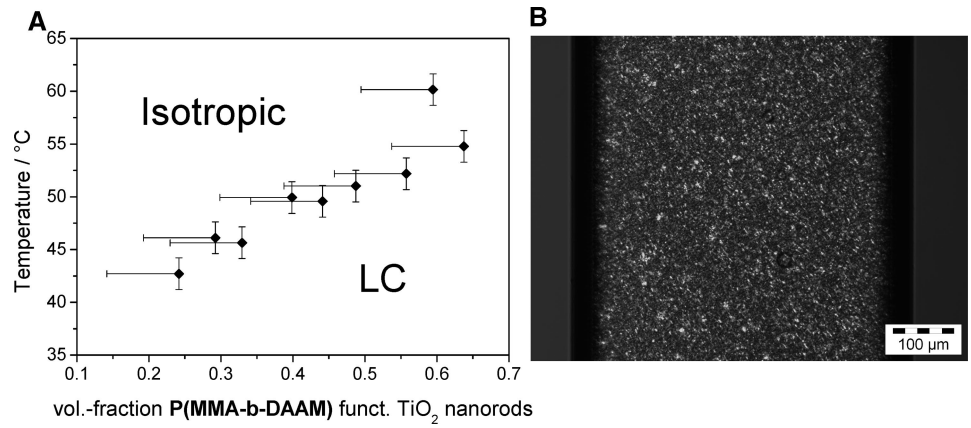


**Figure 5.** (A) Phase diagram of P(MMA-DAAM)-functionalized $TiO_2$ nanorods in PEG 400; (B) liquid crystal phase of 0.65 vol fraction P(MMA-DAAM)-functionalized nanorods in PEG 400; capillary at 25 °C.

The effect of grafting density and molecular weight of the soluble block can be seen in Figure 4. The position of the second zone (the onset of dispersion instability) shifts from 19 °C P(DEGMEMA-*b*-DAAM) **1** to 20 °C for P(DEGMEMA-*b*-DAAM) **2**. This effect can be explained by the molecular weight difference of the two polymers.[33] The difference in the hydrodynamic radius can be rationalized by the difference in the molecular weight between P(DEGMEMA-*b*-DAAM) **1** and **2** in combination with the lower grafting density of P(DEGMEMA-*b*-DAAM) **2**: In cold water, it is around 75 nm for P(DEGMEMA-*b*-DAAM) **1** and 100 nm for P(DEGMEMA-*b*-DAAM) **2**.

## Liquid Crystalline Phases

**PMMA-Functionalized $TiO_2$ Nanorods in PEG 400.** We had previously observed thermotropic phases from polymer-functionalized $TiO_2$ nanorods,[18] whereas only lyotropic (i.e., concentration dependent) phase formation is expected due to hard-core interactions. Thus, we wanted to investigate this effect. We focused on P(MMA-*b*-DAAM) and P(DEGMEMA-*b*-DAAM) **1**-stabilized nanorods, which have similar hydrodynamic radii, for the investigation of their liquid crystalline self-organization. For a thermal investigation of the liquid crystalline behavior of PMMA-functionalized nanorods, a high boiling organic solvent is needed. It must, of course, be a suitable solvent for the polymer shell and should withstand more than 150 °C. PEG 400 (oligomers with approximately 10 repeat units) and PMMA are well miscible,[34] and in first experiments a liquid crystalline phase could be found.[18] Here, we investigated the concentration dependency on the clearing temperature by differential scanning calorimetry (DSC) and polarized optical microscopy. We prepared a set with a constant amount of $TiO_2$ nanorods and a various amount of PEG 400 in THF solution. The samples were then filtered and concentrated in a DSC pan. In addition, we used this solution to fill glass capillaries and allowed the THF to evaporate. Thus, we can analyze the samples in DSC as well as in polarized microscopy (equipped with a heating stage). The temperatures found match well, and the results are shown in Figure 5A. (The temperature error bars resemble the typical broadness of the transition (around 10 °C). The concentration error bar is due to the fact that filtration loss is occurring.) A typical image of a filled glass capillary is shown in Figure 5B. The texture looks smectic like, and in a former work[18] we used $TiO_2$ nanorods of a broader size distribution where we found a narrow nematic and broad smectic phases. The batch of nanoparticles used this time had less very large rods. Obviously, this leads to disappearance of the nematic phase.

At first, all samples show clearly a reversible temperature-dependent phase transition. This is a consequence of the polymer corona, which creates a soft interaction potential due to steric stabilization. In addition, the clearing temperature from liquid crystalline to isotropic shows a clear concentration dependency: With increasing volume fraction of the nanorods, the clearing temperature rises. As the polymer-coated nanorods pack closer, their interaction increases, which stabilizes the liquid crystalline phase. The boundaries of this phase diagram are a volume fraction of 0.77 (cubic dense packing of cylinders with half-sphere end caps and aspect ratio of 5.5), which corresponds to a dense packing of the rods and a volume fraction of 0.2, below which we could not observe a liquid crystalline phase.

**PDEGMEMA-Functionalized $TiO_2$ Nanorods in Excess PDEGMEMA.** As PDEGMEMA is a polymer with a low $T_g$ and is therefore mobile at room temperature, we prepared samples with excess P(DEGMEMA-*b*-DAAM) **1** as "solvent" and investigated their liquid crystalline behavior. We prepared two samples with 20 and 50 vol % of functionalized nanorods in THF solution. The samples were then filtered, and the THF was removed and investigated by DSC as well as by polarized microscopy. We found again liquid crystalline phases for both, and the observed transition temperatures were 80 and 95 °C. With this example, we could show that the principle of using excess polymer as solvent to form a liquid crystalline phase works. In Figure 6, the liquid crystalline phase of P(DEGMEMA-*b*-DAAM) **1**-functionalized nanorods in excess P(DEGMEMA-*b*-DAAM) **1** is shown.

Figure 6A shows a sample (20 vol % nanorods) that demixes upon heating into a nanorod-rich phase (lower left corner) and a nanorod-poor phase (upper right corner). This biphasic demixing is well-known for dispersed rigid-rod objects and shows nicely the concentration dependency of the lyotropic liquid crystal. A liquid crystalline phase with the larger volume percent of nanorods (50) is shown in Figure 6B.

## Conclusion

We were able to show that it is possible to functionalize $TiO_2$ nanorods with dopamine-functionalized diblock copolymers. After functionalization, it is possible to stably disperse the nanorods successfully in organic solvents. Light scattering proved that the nanorods were dispersed as single objects, and we could use AFM (tapping mode) to visualize the homogeneous polymer shell around the nanorods. The PDEGMEMA-functionalized nanorods showed a temperature-dependent dispersion stability. The dispersions became microscopically (light

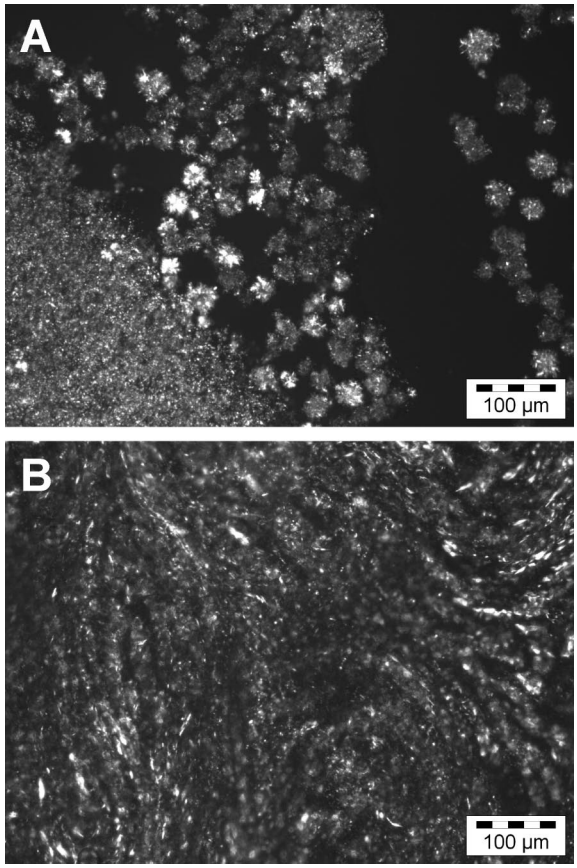


**Figure 6.** Liquid crystalline phase of P(DEGMEMA-*b*-DAAM) **1**-functionalized $TiO_2$ nanorods in excess P(DEGMEMA-*b*-DAAM) **1**: (A) 0.2, (B) 0.5 vol fraction of nanorods.

scattering) and macroscopically (turbidity measurement) unstable when reaching the LCST of PDEGMEMA.

After careful investigations of the nanorod mesogens, we investigated the liquid crystalline phase. The phase diagram of PMMA-functionalized nanorods in PEG 400 was explored, and we found, as one would expect, a rising clearing temperature with increasing volume fraction of nanorods. On the other hand, we investigated PDEGMEMA-functionalized nanorods in excess PDEGMEMA polymer as "solvent" and found again liquid crystalline phases.

## Experimental Section

Methyl methacrylate and styrene (from Acros) and (diethylene glycol monomethyl ether) methacrylate ((2-methoxy-ethoxy)-ethyl methacrylate, from Aldrich) were distilled before usage. Benzyl dithiobenzoate (RAFT reagent)[35] and pentafluorophenol acrylate[27] were synthesized as described in the literature. αα′-Azoisobutyronitrile (AIBN, from Fluka) was recrystallized from diethyl ether. Dopamine hydrochloride (3-hydroxytyramine hydrochloride, from Acros) was used as purchased. Dioxane and tetrahydrofuran (THF) was dried and distilled before usage. All other solvents were also distilled before use. Gel permeation chromatography (GPC) was carried out in THF as solvent, and the detector system contained refractive index (Jasco), UV−vis (Jasco), and light scattering (Wyatt) detectors. Thermogravimetry was carried out in a Perkin-Elmer Pyris 6 TGA under nitrogen atmosphere. NMR spectra were obtained in a Bruker AC 300. AFM images were taken with a Multimode (Nanscope 2a Controller, Veeca St. Barbara) employing an AC 160 Cantilever (Olympus, Germany).

Static light scattering (SLS) measurements were performed with an ALV-SP86 goniometer, an ALV-3000 correlator, a Uniphase HeNe laser (25 mW output power at $\lambda = 632.8$ nm wavelength), and ALV/High QE APD avalanche diode fiber optic detection system. For dynamic light scattering (DLS), an ALV-SP125 goniometer, an ALV-5000 correlator, and a Spectra Physics 2060 argon ion laser (500 mW output power at $\lambda = 514.5$ nm wavelength) were utilized. The scattered intensity was divided by a beam splitter (approximately 50:50), each portion of which was detected by a photomultiplier. The two signals were cross-correlated to eliminate non-random electronic noise.

The complex solutions were typically measured from 30° to 150° in steps of 5° (SLS) or in steps of 10° (DLS). The static scattering intensities were analyzed according to standard procedures to yield the weight average molar mass, $M_w$, and the mean square radius of gyration, $R_g = \sqrt{\langle R_g^2 \rangle_z}$. The correlation functions showed a monomodal decay and were fitted by a sum of two exponentials, from which the first cumulant $\Gamma$ was calculated. The *z*-average diffusion coefficient $D_z$ was obtained by extrapolation of $\Gamma/q^2$ to $q = 0$, leading to the inverse *z*-average hydrodynamic radius $R_h = \langle R_h^{-1} \rangle_z^{-1}$ by formal application of Stokes law. Prior to being mixed, the homopolymer solutions were filtered through 0.2 $\mu$m pore size Dimex filters (Millipore LG) into 20 mm diameter quartz cuvettes (Hellma).

Synthesis of $TiO_2$ nanorods: The synthesis of $TiO_2$ nanorods was carried out using the method reported in ref 18.

Synthesis of P(MMA-*b*-DAAM): First, the macro chain transfer agent (macro-CTA) was synthesized as follows: 2 g (20 mmol) of methyl methacrylate, 112 mg (0.4 mmol) of (4-cyanopentanoic acid)-4-dithiobenzoate, and 8 mg ($5 \times 10^{-5}$ mol) of AIBN were added in a Schlenk tube, and oxygen was exchanged by nitrogen by five freeze−pump−thaw cycles. Polymerization was carried out at 90 °C for 14 h. The macro-CTA was purified by dissolving in THF and precipitating in methanol three times to yield 1.25 g (62%). $M_n$ (MALDI-TOF) = 8500 g/mol, PDI (MALDI-TOF) = 1.07. Second, the reactive diblock copolymer was synthesized: 0.5 g ($5.9 \times 10^{-5}$ mol) of the macro-CTA, 0.5 g (2 mmol) of pentafluorophenole acrylate, and 1 mg ($6 \times 10^{-6}$ mol) of AIBN were added to 2 mL of dioxane in a Schlenk tube. Oxygen was exchanged by nitrogen by five freeze−pump−thaw cycles, and polymerization was carried out at 90 °C for 16 h. The diblock copolymer was purified by dissolving in THF and precipitating in hexane three times to yield 0.55 g. Third, the reactive diblock copolymer was transformed to the polymer ligand P(MMA-*b*-DAAM): 0.55 g ($4 \times 10^{-5}$ mol) of reactive diblock copolymer, 0.25 g (1.2 mmol) of dopamine hydrochloride, and 0.12 g (1.2 mmol) of triethylamine were dissolved in 2 mL of THF and stirred at room temperature overnight. The solution was filtered to remove the triethylamine hydrochloride and precipitated in hexane to yield 0.33 g (67%) of P(MMA-*b*-DAAM). $M_n$ (GPC) = 12 800 g/mol, PDI (GPC) = 1.17. $^1$H NMR (300 MHz, 4:1 *d*-acetone:D-methanol): $\delta$[ppm] 6.7−6.3 (m, 3H, Ph−*H*), 3.59 (s, 3H, O−C*H*$_3$), 2.2−1.7 (m, 5H, [−C*H*$_2$−C*H*R−]$_n$ and [−C*H*$_2$−CRMe−]$_n$), 1.6−0.6 (m, 3H, [−CH$_2$−CR(C*H*$_3$)−]$_n$).

Synthesis of P(DEGMEMA-*b*-DAAM) **1** and **2**: The procedure is the same as that for P(MMA-*b*-DAAM). For the first step, (a) PDEGMEMA **1**, 2 g (10.6 mmol) of (2-methoxy-ethoxy)-ethyl methacrylate, 0.6 g ($1.1 \times 10^{-4}$ mol) of (4-cyanopentanoic acid)-4-dithiobenzoate, and 14.5 mg ($9 \times 10^{-5}$ mol) of AIBN and (b) PDEGMEMA **2**, 2 g (10.6 mmol) of (2-methoxy-ethoxy)-ethyl methacrylate, 0.3 g ($5.4 \times 10^{-5}$ mol) of (4-cyanopentanoic acid)-4-dithiobenzoate, and 2.2 mg ($1.4 \times 10^{-5}$ mol) of AIBN polymerized at 90 °C for 5.5 h. Purification by dissolving in ethyl acetate and precipitating in petrol ether (three times) to yield (a) PDEGMEMA **1**, 1.1 g (55%). $M_n$ (GPC) = 8100 g/mol, PDI (GPC) = 1.15. (b) PDEGMEMA **2**, 1.3 g (65%). $M_n$ (GPC) = 35 000 g/mol, PDI (GPC) = 1.28. $^1$H NMR (300 MHz, $CDCl_3$): $\delta$[ppm] 4.4−3.2 (m, 11H, −C*H*$_2$−C*H*$_2$−O−C*H*$_2$−C*H*$_2$−O−C*H*$_3$), 2.0−1.6 (m, 2H, [−C*H*$_2$−CRMe−]$_n$), 1.3−0.7 (m, 3H, [−CH$_2$−CR(C*H*$_3$)−]$_n$). For the second step, (a) P(DEGMEMA-*b*-DAAM) **1**, 1.1 g ($1.3 \times 10^{-4}$ mol) of the macro-CTA was added to 0.58 g (2.4 mmol) of pentafluorophenole acrylate and 1 mg ($6 \times 10^{-6}$ mol) of AIBN in 2 mL of dioxane; (b) P(DEGMEMA-*b*-DAAM) **2**, 0.5 g ($1.3 \times 10^{-4}$ mol) of the macro-CTA was added to 0.21 g ($8.8 \times 10^{-4}$ mol) of pentafluorophenole acrylate and 0.6 mg ($4 \times 10^{-6}$ mol) of

AIBN in 2 mL of dioxane. Polymerization was carried out at 70 °C for 17 h. For the third step, the reactive diblock copolymers were directly reacted with 10-fold excess dopamine hydrochloride and triethylamine (1: 1) in 2 mL of THF. After filtration, the polymer solution was precipitated in petrol ether to yield (a) P(DEGMEMA-*b*-DAAM) **1**, 0.97 g (58%), $M_n$ (GPC) = 7900 g/mol, PDI (GPC) = 1.25. (b) P(DEGMEMA-*b*-DAAM) **2**, 0.44 g (62%), $M_n$ (GPC) = 47 500 g/mol, PDI (GPC) = 1.53. $^1$H NMR (300 MHz, $CDCl_3$): $\delta$[ppm] 6.7−6.3 (m, 3H, Ph−*H*), 4.4−3.2 (m, 11H, −C*H*−C$H_2$−O−C$H_2$−C$H_2$−O−C$H_3$), 2.9−2.5 (m, 4H, −NH−C$H_2$−C$H_2$−Ph(OH)$_2$), 2.0−1.5 (m, 5H, [−C*H*−CRMe−]$_n$ and [−C$H_2$−C*H*R−]$_n$), 1.3−0.7 (m, 3H, [−CH$_2$−CR(C$H_3$)−]$_n$).

**Acknowledgment.** We would like to thank the "Fonds der chemischen Industrie" and the "Graduate school of excellence: Materials Science in Mainz" for having funded this work (stipend for S.M.). $TiO_2$ nanorods were synthesized and kindly donated by S. Frank working for Prof. W. Tremel (Institute for Inorganic and Analytical Chemistry at the University of Mainz).

**Supporting Information Available:** Calculations used for the light scattering of polydisperse nanorods relating the $\langle R_g^2\rangle_z^{1/2}$ and $\langle 1/R_h\rangle_z^{-1}$ to $\langle L_n\rangle$. This material is available free of charge via the Internet at http://pubs.acs.org.

## References and Notes

(1) Stegemeyer, M., Guest Ed. *Liquid Crystals*; Steinkopf/Springer: Darmstadt/Germany/New York, 1994. Demus, D.; Goodby, J.; Gray, G. W.; Spiess, H.-W.; Vill, V. *Handbook of Liquid Crystals*; Wiley-VCH: Weinheim, Germany, 1998.
(2) Ballauff, M. *Angew. Chem.* **1989**, *101*, 261.
(3) Noël, C.; Navard, P. *Prog. Polym. Sci.* **1991**, *16*, 55.
(4) Davidson, P.; Gabriel, J. C. P. *Curr. Opin. Colloid Interface Sci.* **2005**, *9*, 377.
(5) (a) Flory, P. J. *Proc. R. Soc. London, Ser. A* **1956**, *254*, 73. (b) Flory, P. J.; Ronca, G. *Mol. Cryst. Liq. Cryst.* **1979**, *54*, 289.
(6) Petekidis, G.; Vlassopoulos, D.; Fytas, G.; Kountourakis, N. *Macromolecules* **1997**, *30*, 919–931.
(7) Graetzel, M. *Inorg. Chem.* **2005**, *44*, 6841–6851.
(8) Suri, P.; Mehra, R. M. *Sol. Energy Mater. Sol. Cells* **2007**, *91*, 518–524.
(9) Beek, W. J. E.; Wienk, M. M.; Janssen, R. A. J. *Adv. Mater.* **2004**, *16*, 1009–1013.
(10) Sites, J.; Pan, J. *Thin Solid Films* **2007**, *515*, 6099–6102.
(11) Sudeep, P. K.; Emrick, T. *Polym. Rev.* **2007**, *47*, 155–167.
(12) Huynh, W. U.; Dittmer, J. J.; Alivisatos, A. P. *Science* **2002**, *295*, 2425–2427.
(13) Zocher, H. *Z. Anorg. Allg. Chem.* **1925**, *147*, 91.
(14) Brunello, C. A.; Graeff, C. F. O. *J. Non-Cryst. Solids* **2002**, *304*, 265.
(15) Bawden, F. C.; Pirie, N. W.; Bernal, J. D.; Fanhucken, I. *Nature* **1936**, *138*, 1051.
(16) (a) Dessombz, A.; Chiche, D.; Davidson, P.; Panine, P.; Chanéac, C.; Jolivet, J.-P. *J. Am. Chem. Soc.* **2007**, *129*, 5904. (b) Michot, L. J.; Bihannic, I.; Maddi, S.; Baravian, C.; Levitz, P.; Davidson, P. *Langmuir* **2008**, *24*, 3127.
(17) (a) Tahir, M. N.; Zink, N.; Eberhardt, M.; Therese, H. A.; Kolb, U.; Theato, P.; Tremel, W. *Angew. Chem.* **2005**, *45*, 4809. (b) Tahir, M. N.; Eberhardt, M.; Theato, P.; Faiss, S.; Janshoff, A.; Gorelik, T.; Kolb, U.; Tremel, W. *Angew. Chem., Int. Ed.* **2006**, *45*, 908.
(18) (a) Meuer, S.; Oberle, P.; Theato, P.; Tremel, W.; Zentel, R. *Adv. Mater.* **2007**, *19*, 2073–2078. (b) Zorn, M.; Meuer, S.; Tahir, M. N.; Khalavka, Y.; Sönnichsen, C.; Tremel, W.; Zentel, R. *J. Mater. Chem.* **2008**, *18*, 3050–3058.
(19) (a) Li, L.; Walda, J.; Manna, L.; Alivisatos, A. P. *Nano Lett.* **2002**, *2*, 557. (b) Lemaire, B. J.; Davidson, P.; Ferre, J.; Jamet, J.; Petermann, D.; Panine, P.; Dozov, I.; Stoenescu, D.; Jolivet, J. *Faraday Discuss.* **2005**, *128*, 271.
(20) (a) He, J.; Zhang, Q.; Gupta, S.; Emrick, T.; Russell, T. P.; Thiyagarajan, P. *Small* **2007**, *3*, 1214–1217. (b) Jana, N. R. *Chem. Commun.* **2003**, *15*, 1950.
(21) (a) Zhang, Z. X.; van Duijneveldt, J. S. *J. Chem. Phys.* **2006**, *124*, 154910. (b) Leach, E. S. H.; Hopkinson, A.; Franklin, K.; van Duijneveldt, J. S. *Langmuir* **2005**, *21*, 3821.
(22) (a) van der Beek, D.; Reich, H.; van der Schoot, P.; Dijkstra, M.; Schilling, T.; Vink, R.; Schmidt, M.; van Roij, R.; Lekkerkerker, H. N. W. *Phys. Rev. Lett.* **2006**, *97*, 087801. (b) van Bruggen, M. P. B.; van der Kooij, F. M.; Lekkerkerker, H. N. W. *J. Phys.: Condens. Matter* **1996**, *8*, 9451.
(23) (a) Sciancalepore, C.; Cassano, T.; Curri, M. L.; Mecerreyes, D.; Valentini, A.; Agostiano, A.; Tommasi, R.; Striccoli, M. *Nanotechnology* **2008**, *19*, 205705. (b) Convertino, A.; Leo, G.; Tamborra, M.; Sciancalepore, C.; Striccoli, M.; Curri, M. L.; Agostiano, A. *Sens. Actuators, B* **2007**, *126*, 138–143.
(24) (a) Meuer, S.; Braun, L.; Zentel, R. *Chem. Commun.* **2008**, *27*, 3166–3168. (b) Lou, X.; Daussin, R.; Cuenot, S.; Duwez, A.-S.; Pagnoulle, C.; Detrembleur, C.; Bailly, C.; Jérômev, R. *Chem. Mater.* **2004**, *16*, 4005–4011. (c) Bahun, G. J.; Wang, C.; Adronov, A. *J. Polym. Sci., Part A: Polym. Chem.* **2006**, *44*, 1941.
(25) Zorn, M.; Zentel, R. *Macromol. Rapid Commun.* **2008**, *29*, 922–927.
(26) Moad, G.; Rizzardo, E.; Thang, S. H. *Aust. J. Chem.* **2005**, *58*, 379–410.
(27) (a) Eberhardt, M.; Theato, P. *Macromol. Rapid Commun.* **2005**, *26*, 1488. (b) Eberhardt, M.; Mruk, R.; Zentel, R.; Theato, P. *Eur. Polym. J.* **2005**, *41*, 1569–1575.
(28) Lee, H.; Lee, B. P.; Messersmith, P. B. *Nature* **2007**, *448*, 338–342.
(29) Xu, C.; Xu, K.; Gu, H.; Heng, R.; Liu, H.; Zhang, X.; Guo, Z.; Xu, B. *J. Am. Chem. Soc.* **2004**, *126*, 9938.
(30) (a) Rajh, T.; Chen, L. X.; Lukas, K.; Liu, T.; Thurnauer, M. C.; Tiede, D. M. *J. Phys. Chem. B* **2002**, *106*, 10543. (b) de la Garza, L.; Saponjic, Z. V.; Dimitrijevic, N. M.; Thurnauer, M. C.; Rajh, T. *J. Phys. Chem. B* **2006**, *110*, 680.
(31) (a) Schmidt, M. *Macromolecules* **1984**, *17*, 553–560. (b) Oberthuer, R. C. *Makromol. Chem.* **1978**, *179*, 2693–2706.
(32) Broersma, S. *J. Chem. Phys.* **1960**, *32*, 1632.
(33) Han, S.; Hagiwara, M.; Ishizone, T. *Macromolecules* **2003**, *36*, 8312–8319.
(34) Ito, H.; Russell, T. P.; Wignall, G. D. *Macromolecules* **1987**, *20*, 2213–2220.
(35) Chong, Y. K.; Krstina, J.; Le, T. P. T.; Moad, G.; Postma, A.; Rizzardo, E.; Thang, S. H. *Macromolecules* **2003**, *36*, 2256.

MA801369W